Strong enhancement of the radiative decay rate of emitters by single plasmonic nanoantennas.

O. L. Muskens,[1] V. Giannini,[2] J. A. Sánchez-Gil,[2] and J. Gómez Rivas[1]

[1]*FOM Institute for Atomic and Molecular Physics AMOLF, c/o Philips Research Laboratories,*
High Tech Campus 4, 5656 AE, Eindhoven, The Netherlands.
[2]*Instituto de Estructura de la Materia, Consejo Superior de Investigaciones Científicas, Serrano 121, 28006 Madrid, Spain*
(Dated: July 27, 2007)

We demonstrate a strong, fivefold enhancement of the radiative decay rate from highly-efficient fluorescent dye molecules around resonant optical nanoantennas. The plasmonic modes of individual gold dimer antennas are tuned by the particle length and the antenna gap, providing control over both the spectral resonance position and the near-field mode profile of the nanoantenna. Resonant enhancement of the radiative and nonradiative decay rates of a fluorescent dye is observed, resulting in an increase of the internal quantum efficiency from 40% up to 53% for single antennas, and up to 59% for antenna clusters. This improvement of the already high quantum efficiency of the dye molecules is in agreement with electrodynamic model calculations that predict a maximum attainable efficiency around 80% due to nonradiative losses in the metal.

In recent years there has been an enormous interest in plasmonic nanostructures for applications in biosensing, nanophotonics, and enhanced light emission.[1, 2] Surface plasmons give rise to large local field enhancements which may be used for nonlinear optical spectroscopy such as SERS, multiphoton absorption, and for enhancement of fluorescence. Although many studies have addressed the enhancement of fluorescence, it has turned out extremely difficult to selectively enhance only the radiative decay channels using plasmons. Selective modification of only radiative decay channels is crucial for light-emitting devices that benefit only from radiative enhancement. The further improvement of highly efficient emitters with nanostructures in general, and specifically with plasmonic nanostructures, represents a scientific challenge with important technological consequences.

For rough metal films, extremely large (up to 10^3) increases in intrinsic relaxation rates were reported, which were however governed by nonradiative losses in the metal.[3, 4] Recent investigations on small metal nanoparticles[5–8] have lead to significant advancements in the understanding of the effect of emitter-particle distance on the fluorescence yield. Various other geometries have been under investigation recently, including nanoshells[9] and lithographic particle arrays with various shapes and sizes.[10, 11] Although in many cases an increase of the total fluorescence intensity has been observed, a large portion of this has to be attributed to enhancement of excitation rates. The few reports in which effects on the excitation and spontaneous emission could be unambiguously separated experimentally[3, 7, 11] showed a predominant enhancement of nonradiative decay rates and hence a quenching of fluorescence emission.

From the above investigations the crucial picture emerges that the most critical step in plasmon-enhanced fluorescence emission is not the coupling of the emitter to plasmonic modes, but rather the efficient radiative outcoupling of surface plasmons into photons. We investigate here a novel class of nanoparticle designs that are optimized specifically with respect to this radiative outcoupling of plasmons into far-field light. These so-called optical antennas have recently been proposed based on analogies with radiowave antennas[12, 13], and combine a high radiative efficiency with strong geometric resonances and large local field enhancement in the gap between two interacting nanoparticles. This strong improvement of the matching of far-field optical radiation with local dipoles makes optical antennas extremely promising elements for nonlinear spectroscopy[12, 13] and for extraction of light from emitters.[14, 15]

In order to conclusively identify the different contributions to the plasmon enhanced fluorescence, we combine in our experiment several key elements, namely: (i) precise variation of relevant antenna parameters, (ii) detailed knowledge of the plasmonic mode spectrum, (iii) separation between plasmonic effects in the excitation and emission rates, and (iv) extraction of intensities and decay rates using fluorescence lifetime imaging. In contrast to previous reports in which low quantum-yield emitters were used[9, 10], we choose as starting point a dye with a relatively high quantum efficieny of 40% (Atto680, Atto Tec GmbH). The large Stokes shift of ~ 70 nm of this dye allows a separate treatment of excitation and emission rate effects in the fluorescence.

We specifically consider dimer antennas, consisting of two rod-shaped arms, since these are the simplest realization of a rich diversity of potential nanoantenna structures. Several experimental and theoretical investigations have shown that extended-size nanorods act as standing-wave resonators for surface plasmon polaritons, exhibiting geometrical half-wavelength resonances with spectral positions depending strongly on antenna arm length.[13, 16–18] We unambiguously show here that the coupling between the two antenna arms results in an improved average response of the antenna-emitter complex compared to resonant antennas with uncoupled arms. We
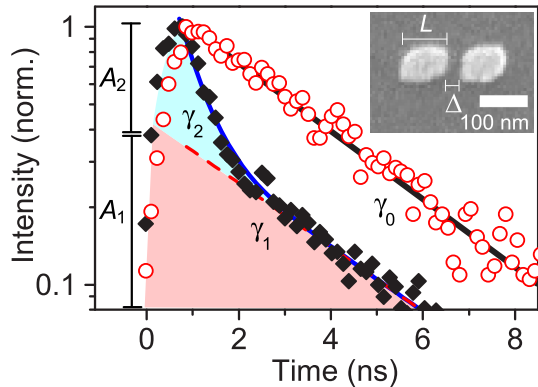
FIG. 1: Normalized fluorescence decay measured at a resonant nanoantenna (diamonds, black) and away from the nanoantenna (open dots, red), with exponential decay fits (lines, black). Inset: SEM image of the resonant gold nanoantenna, consisting of two $90 \times 60 \times 20$ nm^3 gold nanorods with an antenna gap of 20 nm.
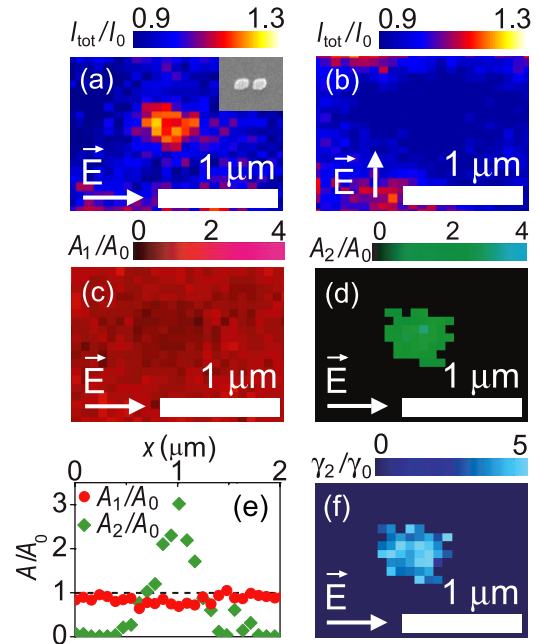

FIG. 2: (a) Fluorescence intensity around a single resonant gold nanoantenna [on-scale SEM image in inset of (a)], for polarization of the detected light parallel, and (b) perpendicular to the antenna axis. Scale bars denote 1 μm. (c,d) Double-exponential fitted amplitudes for slow and fast decay components A_1 and A_2, normalized to value A_0 in absence of antenna, for parallel emission polarization. (e) Horizontal cross-sections of Figs. 1(b,c). (f) Fast decay component γ_2 normalized to γ_0.

find that, while the linear scattering spectra are very similar, the decay rate enhancements show a pronounced difference, which clearly demonstrates the importance of the near-field mode profile besides the spectral resonance structure. We also present rigorous calculations of the decay rate of a dipole in the proximity of the nanoantenna, which are in qualitative agreement with the measurements. These calculations predict a limit to the enhancement related to nonradiative losses in the metal.

Arrays consisting of individual gold nanoantennas of 20 nm thickness were fabricated using e-beam lithography.[19] Subsequently, a 10 ± 2-nm silica spacer layer was deposited, followed by an active layer of 10 nm thickness fabricated by spincoating of a concentration (3×10^{-5} M) of dye molecules embedded in a polymer (PVB) matrix. The selected dye concentration resulted in a coverage of several hundred dye molecules per μm^2. The highly photostable dye has a fluorescence decay time of 3.3 ns with a corresponding quantum efficiency η of 40% in ethanol, and emits in a spectral band around 730 nm. A scanning electron microscopy (SEM) image of a dimer nanoantenna consisting of two $90 \times 60 \times 20$ nm^3 antenna arms with an antenna gap, Δ, of 20 nm is shown as an inset of Fig. 1.

The fluorescence lifetimes of dye molecules deposited around single nanoantennas were measured using a time-correlated single-photon counting setup[20] (Picoquant GmbH) synchronized with a laser-scanning confocal microscope (Nikon C1). In this setup the fluorescence decay as a function of time was measured while spatially scanning the excitation laser beam over the sample. The molecules were excited by light from pulsed diode laser with 150 ps pulse duration, polarized parallel to the antenna long axis. The pump beam was focused to a near-diffraction limited spot of less than 0.5 μm by means of a $100\times$, 0.9 N.A., microscope objective, resulting in an energy per pulse of $\sim$50 μJ/cm^2 on the sample. Note

that the excited volume is still considerably larger than a single nanoantenna. Emitted fluorescence photons were collected using the same 0.9 N.A. microscope objective and detected by means of a photon-counting avalanche diode. Figure 1 shows fluorescence decay curves taken at the position of a resonant nanoantenna (diamonds, black) and more than 1 μm away from the antenna (circles, red). In absence of an antenna, the decay is single-exponential with a decay rate, γ, identical to the value measured in ethanol, $\gamma_0 = 0.3$ ns^{-1}. At the position of the antenna, the fluorescence decay is multi-exponential with a slow component, γ_1, equal to γ_0. We attribute this slow component, indicated by the red area in Fig. 1, to a background of dye molecules in the excited volume that do not couple to the antenna. The fast component can be fitted to an exponential with a decay rate, γ_2, of 1.7 ns^{-1}, more than five times larger than γ_0. We assign this contribution, indicated by the blue area in Fig. 1, to a fraction of molecules that is coupled to the nanoantenna.

A complete spatial and temporal image of fluorescence decay around single nanoantennas was obtained from two-dimensional scans, in which time-resolved fluorescence decay curves like those in Fig. 1 were measured at several positions. Typical results for a resonant antenna are presented in Fig. 2. Figure 2(a) shows an image of the total fluorescence intensity, I_{tot} emitted with a polar-

ization parallel to the nanoantenna long axis, normalized to the average intensity I_0 far away from any antenna. We observe an increase of the intensity to 1.3 times I_0 at the position of the nanoantenna. For polarization of the emitted light perpendicular to the antenna, shown in Fig. 2(b), no increase is observed. Since the polarization of the excitation light remained fixed, this indicates that the increase of the fluorescence intensity is related to the emission properties of the antenna-coupled dye fraction and not just to an enhancement of the pump intensity. The corresponding time-resolved fluorescence curves have been fitted to a double exponential decay function

$$I(t) = A_1 e^{-\gamma_1 t} + A_2 e^{-\gamma_2 t}, \tag{1}$$

yielding the amplitudes A_1, A_2 and decay rates γ_1, γ_2 for the slow and fast decay components, respectively. The amplitudes are shown in Figs. 2(c,d), normalized to the single-exponential background amplitude in absence of the antenna, denoted by A_0. The increase of A_2 and reduction of A_1 around the nanoantenna are also represented in Fig 2(e) where a horizontal line scan of Figs. 2(c) and (d) across the middle of the nanoantenna is shown. The fast component A_2 increases to three times the background A_0 within a near-diffraction limited spot with a diameter of ~ 0.5 μm. The slow component A_1 decreases to around $0.8 A_0$, indicating that only a relatively small fraction of molecules ($\sim 20\%$) in the diffraction-limited spot couples to the nanoantenna. The fast decay rate γ_2, shown in Fig. 2(f), is only present around the nanoantenna, where we observe a five-fold reduction of the lifetime.

From the experimental values of the intensities and fluorescence decay rates, we can obtain the corresponding radiative and nonradiative components by making one justified assumption, namely, we estimate an average quantum efficiency enhancement η/η_0 from the local intensity ratio I_{tot}/I_0. By doing this we assume that no contributions are present from pump field enhancement. This assumption is justified by the polarization-dependence of the intensity enhancement in Figs. 2(a,b) and by the low, nonresonant scattering at the pump wavelength as observed in Fig. 3(a,b) (diamonds, green), as will be discussed below. The definition of the quantum efficiency in terms of the ratio of the radiative to the total decay rate $\eta = \gamma_R/\gamma_{\text{tot}}$ can be inverted, yielding $\gamma_R = \eta \gamma_{\text{tot}}$ and $\gamma_{NR} = (1 - \eta)\gamma_{\text{tot}}$. For the dye molecules coupled to the antenna, the experimental total decay rate γ_{tot} equals γ_2. In the final analysis, each parameter is averaged over eight identically designed antennas to reduce variations due to the local distribution and orientations of dye molecules.

We measured the fluorescence decay for single nanoantennas with various arm lengths L, for the two cases of strongly coupled arms (gap width $\Delta = 20$ nm) and virtually uncoupled arms ($\Delta > 80$ nm). Figures 3(c,d) show the resulting values of γ_R (open circles) and γ_{NR} (closed diamonds), relative to their values in absence of the metal structures, for the two cases of strongly coupled (c) and
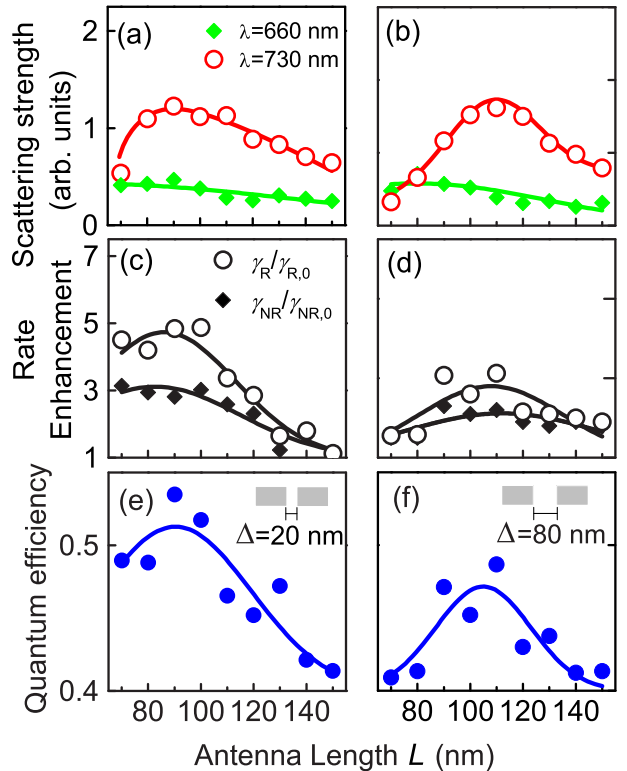

FIG. 3: Analysis of coupled (a,c,e) and uncoupled (b,d,f) nanoantennas, respectively with antenna gap widths of $\Delta = 20$ nm and $\Delta > 80$ nm, against antenna arm length L. (a,b) Scattering strength at the excitation ($\lambda = 660$ nm, diamonds, green) and emission ($\lambda = 730$ nm, circles, red) wavelengths, for longitudinal polarization. Lines denote calculated cross sections using model calculations (see text).[19] (c,d) Enhancement of the radiative (open dots, black) and nonradiative (diamonds, black) rates γ_R and γ_{NR}. (e,f) Average quantum efficiency. Lines are guides to the eye.

uncoupled (d) antenna arms. For the strongly coupled antenna arms ($\Delta = 20$ nm), a maximum of enhancement occurs for the shortest antennas ($L = 80$ nm). The combined resonant enhancement of both γ_R and γ_{NR} results in an increase of the average quantum efficiency from 40% up to $53 \pm 3\%$ for the resonant antennas with small gap widths, as shown in Fig. 3(e) (circles, blue). For the uncoupled antennas ($\Delta > 80$ nm), the enhancement of both decay rates and of the quantum efficiency is less strong than for the coupled antennas [Fig. 3(f)]. The results of Fig. 3 demonstrate that resonant dimer antennas with strongly coupled arms yield a larger enhancement of spontaneous emission than uncoupled antennas.

In order to relate the observed enhancements to the plasmonic mode structure of the nanoantennas, we have also investigated their spectral response. The antennas are illuminated by a broadband source using a darkfield microscope objective, while the far-field scattered intensity is detected by an avalanche photodiode. A more detailed spectroscopic study of the individual nanoantennas is published elsewhere.[19] A clear longitudinal plasmon
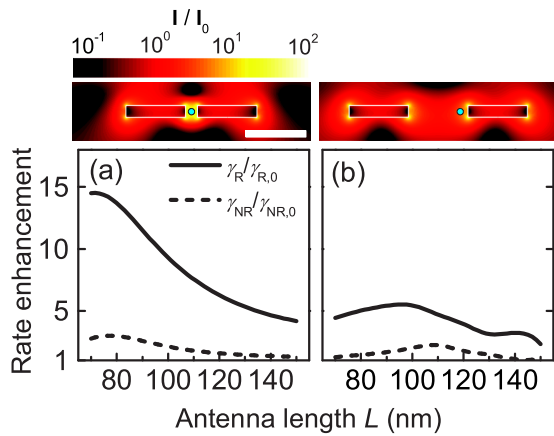
FIG. 4: Modified spontaneous emission calculated for a dipole emitter at 730 nm wavelength, positioned at the location of maximum coupling to the antenna and oriented parallel to the antenna axis. Radiative and nonradiative decay rates γ_R, γ_{NR} are shown versus antenna arm length L, for the two cases of (a) strongly coupled antenna arms ($\Delta = 20$ nm), and (b) uncoupled antenna arms ($\Delta = 80$ nm). (Top graphs) Calculated near-field intensities around two resonant antennas for plane-wave illumination[19], with spots (cyan) indicating the location of the emitter in the calculations (scale bar denotes 100 nm).

resonance occurs for the individual nanoantenna arms that is hybridized for small gap distances when the arms are capacitively coupled.[16, 21] In Fig. 3(a,b) we present measurements of the antenna scattering strengths in the two relevant spectral regions of the fluorescence measurements, namely the excitation wavelength (660 nm, green diamonds) and emission band of the dye (730 nm ±30 nm, red circles). The intensity in the emission band clearly shows a resonant dependence on L corresponding to the shift of the longitudinal surface plasmon mode through the selected spectral window. For the strongly coupled arms ($\Delta = 20$ nm), this resonance is redshifted with respect to the individual particle resonance, leading to a maximum at smaller lengths L.[19] The scattered intensities taken at the excitation wavelength [green diamonds in Fig. 3(a) and (b)] do not show such a resonant behavior since these are located next to the longitudinal plasmon mode. Clearly, both the radiative and nonradiative rates [Fig. 3(c,d)] and the average quantum efficiencies [Fig. 3(e,f)] show a strong correlation with the scattering strength in the emission band. The absence of enhancement for the shortest antennas with $\Delta > 80$ nm validates the assumption of negligible excitation field enhancement.

To model the fluorescence enhancement we have made use of the rigorous scattering equations of the Green's theorem surface integral equations to calculate the local near-field intensity in the corresponding two-dimensional geometries.[19, 23] The result of these calculations are shown in the upper images of Fig. 4. For the strongly coupled antenna arm ($\Delta = 20$ nm), a strong enhance-

ment of the local intensity of up to 10^2 is found in the center of the gap. For extended antenna sizes as those of this study, it has been shown experimentally[17, 18] and theoretically[13, 16] that the longitudinal resonances correspond to a half-wave dipolar mode. This mode profile is considerably different from that of the small spherical particles considered in classical electromagnetic models for fluorescence enhancement.[22]

Next, the scattering formulation is exploited to determine the modification of spontaneous emission of dye molecules by the local plasmonic mode density. This is done by treating them as classical dipoles $\mathbf{p}$, where the total decay rate, $\gamma = \gamma_{NR,0} + \gamma_{NR} + \gamma_R$ (where $\gamma_{NR,0}$ is the intrinsic nonradiative decay rate of the dye), is obtained from the imaginary part of the local, self-consistent electric field $\mathbf{E}_{local}$, through[24]

$$\gamma/\gamma_0 - 1 \propto (\eta_0/|\mathbf{p}|^2)\mathrm{Im}\{\mathbf{p^*} \cdot \mathbf{E}_{local}\}. \qquad (2)$$

$\mathbf{E}_{local}$ is calculated from the rigorous scattering formulation; radiative and non-radiative decay rates are discerned by performing the calculations with and without metal absorption. In Fig. 4(a) and (b) we present results for a dipole positioned at the location in the gap where the largest modification of the spontaneous emission takes place [indicated by a dot in the near-field maps of Fig. 4]. Clearly, both the calculated radiative and nonradiative rates in Fig. 4(a,b) show the same strong dependence on L as seen in the experiments. The calculated enhancements are a factor of 3 higher than the experimental ones, and show a larger difference between radiative and nonradiative components. These differences are due to the fact that the calculations are performed at the point of the maximum field enhancement, while in the experiments we measure the average decay rate close to the antenna. Also, in the experimental analysis we used an ensemble-averaged quantum efficiency which overestimates the nonradiative part in the total decay rate. A complete ensemble calculation would involve a complex averaging over all positions and orientations of molecules, which is beyond the scope of this work.

The positive influence of antenna arm coupling on the total decay rate, observed both experimentally and theoretically, implies a direct modification of the local field enhancement. Our model allows us to attribute this to the formation of a 'hot spot' in the antenna gap and edges, as seen in the corresponding near-field profile of Fig. 4, resulting in an increase of the local density of plasmon modes. The combination of the radiative and nonradiative decay rate enhancements of Fig. 4(a) with the experimental efficiency of the dye results in a maximum achievable internal quantum efficiency of 80%, limited by the intrinsic nonradiative losses in the metal.

To explore the limits of the maximum achievable quantum efficiency with nanorod dimers as presented above, we have increased the fraction of antenna-coupled dye molecules by fabricating clusters of antennas containing up to 4 dimers within a diffraction limited spot size. The resulting average quantum efficiency enhancements
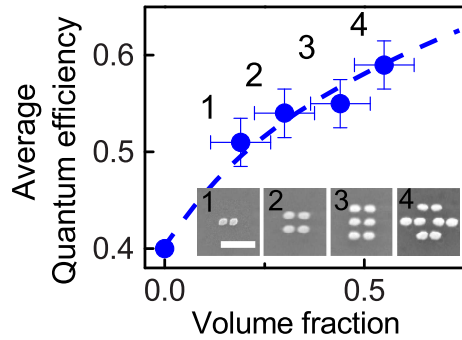
FIG. 5: Average quantum efficiency obtained for different clusters of antennas (numbers indicating amount of antennas), versus the fraction of emitters coupled to the antennas. Line is guide to the eye. Insets: SEM images of antenna clusters, scale bar denotes 500 nm.

for the most resonant antennas with strongly interacting arms (i.e. with parameters $L = 80$ nm and $\Delta = 20$ nm) are shown in Fig. 5 versus the estimated fraction of coupled molecules. The increase of the number of antennas in the cluster up to 4 further improves the quantum efficiency up to 59%. Extrapolation of our measurements to 100% coupled dye fraction points to a maximum achievable quantum efficiency of around 70%, in agreement with the calculated saturation due to nonradiative losses.

In conclusion, we have observed resonant enhancement of light extraction from dye molecules by optical nanoantennas. By designing metal antennas with optimized arm length and gap width, the spontaneous emission of a fluorescent dye was enhanced by more than a factor 5, while the quantum efficiency was improved from 40% to 53% with single nanoantennas. A clear effect of antenna coupling on the spontaneous emission enhancement was found and explained, using a theoretical model, by the strong local field enhancement in the antenna gap. We conclude that, although enhancement is limited by metal losses, these can be small enough to result in considerable quantum efficiency improvement.

[1] Ozbay, E., Science **2006**,311, 189.
[2] Barnes, W. L.; Dereux, A.; Ebbesen, T. W., Nature **2003**, 424, 824.
[3] Gontijo, I.; Boroditsky, M.; Yablonovitch, E.; Keller, S.; Mishra, U. K.; DenBaars, S. P., Phys. Rev. B **1999**, 60, 11564-11567.
[4] Shimizu, K. T.; Woo, W. K.; Fisher, B. R.; Eisler, H. J.; Bawendi, M. G., Phys. Rev. Lett. **2002**, 89, 117401:1-4.
[5] Kulakovich, O.; Strekal, N.; Yaroshevich, A.; Maskevich, S.; Gaponenko, S.; Nabiev, I.; Woggon, U.; Artemyev, M., Nano Lett. **2002**, 2, 1449.
[6] Anger, P.; Bharadwaj, P.; Novotny, L., Phys. Rev. Lett. **2006**, 96, 113002
[7] Kühn, S.; Hakanson, U.; Rogobete, L.; Sandoghdar, V., Phys. Rev. Lett. **2006**,97, 017402.
[8] Dulkeith, E.; Ringler, M.; Klar, T. A.; Feldmann, J.; Munoz Javier, A; Parak, W. J., Nano Lett. **2005**, 5, 585-589.
[9] Tam, F.; Goodrich, G. P.; Johnson, B. R.; Halas, N. J., Nano Lett., **2007**, 7, 496-501.
[10] Biteen, J. S.; Lewis, N. S.; Atwater, H. A.; Mertens, H.; Polman, A., Appl. Phys. Lett. **2006** 88, 131109
[11] Gerber, S.; Reil, F.; Hohenester, U.; Schlagenhaufen, T.; Krenn, J. R.; Leitner, A.; Phys. Rev. B, **2007**, 75, 073404-1:4.
[12] Schuck, P. J.; Fromm, D. P.; Sundaramurthy, A.; Kino, G. S.; Moerner, W. E., Phys. Rev. Lett. **2005**, 94, 017402.
[13] Mühlschlegel, P.; Eisler, H.-J.; Martin, O. J. F.; Hecht, B.; Pohl, D. W., Science **2005**,308, 1607.
[14] Farahani, J. N.; Pohl, D. W.; Eisler, H.-J.; Hecht, B., Phys. Rev. Lett. **2005**, 95, 017402.
[15] Taminiau, T. H.; Moerland, R. J.; Segerink, F. B.; Kuipers, L.; Van Hulst, N. F., Nano Lett. **2007**, 7, 28-33.
[16] Aizpurua J.; Bryant, G. W.; Richter, L. J.; García de Abajo, F. J.; Kelley, B. K.; Mallouk, T., Phys. Rev. B **2005**,71, 235420.
[17] Krenn, J. R.; Schider, G.; Rechberger, W.; Lamprecht, B.; Leitner, A.; Aussenegg, F. R.; Weeber, J. C., Appl. Phys. Lett. **2000**, 77, 3379.
[18] Imura, K.; Nagahara, T.; Okamoto, H., J. Phys. Chem. B **2004**, 108, 16344.
[19] Muskens O. L.; Giannini, V.; Sánchez-Gil, J. A.; Gómez Rivas, J., cond.mat./0612689 (2006).
[20] Lakowicz, J.R., *Principles of fluorescence spectroscopy*, 3rd ed.; Springer: New York, 2006.
[21] Nordlander, P.; Oubre, C.; Prodan, E.; Li, K.; Stockman, M. I., Nano Lett. **4**, 899 (2005).
[22] (a) Ford, G. W.; Weber, W. H., Phys. Rep. **1984**,113, 195. (b) Gersten, J.; Nitzan, A.; J. Chem. Phys. **1981**, 75, 1139.
[23] Sánchez-Gil, J. A.; García-Ramos, J. V.; Méndez, E. R., Phys. Rev. B **2000**, 62, 10515.
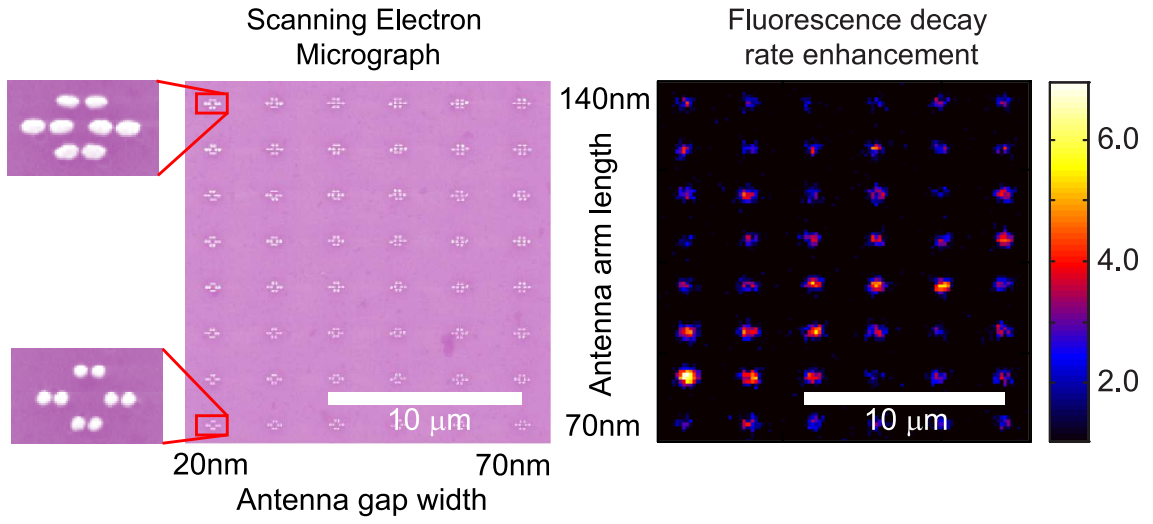[24] Novotny, L., Appl. Phys. Lett. **2005**,69, 3806.

FIG. 6: Table of Contents Figure.